J. Fluid Mech. (2010), *vol.* 649, *pp.* 187–203.
doi:10.1017/S0022112009993405

Testing the limits of quasi-geostrophic theory: application to observed laboratory flows outside the quasi-geostrophic regime

PAUL D. WILLIAMS[1]†, PETER L. READ[2] AND THOMAS W. N. HAINE[3]

[1]Department of Meteorology, University of Reading, Earley Gate, Reading RG6 6BB, UK

[2]Department of Physics, University of Oxford, Parks Road, Oxford OX1 3PU, UK

[3]Department of Earth and Planetary Sciences, 329 Olin Hall, 34th and North Charles Streets, Johns Hopkins University, Baltimore, MD 21218, USA

(Received 3 February 2009; revised 9 November 2009; accepted 9 November 2009)

We compare laboratory observations of equilibrated baroclinic waves in the rotating two-layer annulus, with numerical simulations from a quasi-geostrophic model. The laboratory experiments lie well outside the quasi-geostrophic regime: the Rossby number reaches unity; the depth-to-width aspect ratio is large; and the fluid contains ageostrophic inertia–gravity waves. Despite being formally inapplicable, the quasi-geostrophic model captures the laboratory flows reasonably well. The model displays several systematic biases, which are consequences of its treatment of boundary layers and neglect of interfacial surface tension and which may be explained without invoking the dynamical effects of the moderate Rossby number, large aspect ratio or inertia–gravity waves. We conclude that quasi-geostrophic theory appears to continue to apply well outside its formal bounds.

1. Introduction

Fluid flows observed in the rotating laboratory annulus, and their comparison with numerical simulations, remain an important testbed for investigating many fundamental phenomena in geophysical fluid dynamics (e.g. Hignett *et al.* 1985; Lewis 1992; Williams, Haine & Read 2005; Read *et al.* 2007). The interpretation of laboratory observations in the context of numerical simulations, and *vice versa*, sharpens the existing dynamical questions and raises new ones. The basic formulation of numerical models may be tested much more rigorously and stringently in the context of laboratory fluids than of the atmosphere and ocean because the latter contain much more complexity. Indeed, the prospect of achieving traditional numerical convergence of realistic atmosphere or ocean models may be hopeless because of this complexity (McWilliams 2007).

Numerical models have been developed to integrate the Navier–Stokes equations for the rotating annulus (e.g. White 1986). Although these models contain a complete representation of the fluid dynamics, they are computationally very expensive. In practice, usually they are useful only for examining a small number of case-study flows. It is often desirable to use a faster, approximate model with fewer dynamical

† Email address for correspondence: p.d.williams@reading.ac.uk

degrees of freedom. Quasi-geostrophic numerical models fall into this class and have been developed for the rotating rectangular channel (e.g. Brugge, Nurser & Marshall 1987) and the rotating cylindrical annulus (e.g. Williams *et al.* 2009). There is a tension between accuracy and speed in any computational modelling exercise. Although a Navier–Stokes model would give more faithful simulations than a quasi-geostrophic model, it could take orders of magnitude longer to run. A rapid approximate answer is often preferable to a delayed exact answer.

Quasi-geostrophic theory (Charney, Fjørtoft & von Neumann 1950) formally applies only to flows that are shallow, have small Rossby number and are devoid of ageostrophic motions. But to what extent is quasi-geostrophic theory able to capture the full fluid dynamics, especially in dynamical regimes in which the theory does not formally apply? Very few studies have attempted to answer this critical question. Mundt, Vallis & Wang (1997) reported that their quasi-geostrophic numerical model performs quite well, 'far beyond its expected range of validity' in some cases, compared with a shallow-water equations control run. Zurita-Gotor & Vallis (2009) found that primitive-equation and quasi-geostrophic simulations of the equilibration of baroclinic turbulence agree reasonably well over a fairly broad parameter range. But how applicable is quasi-geostrophic theory to deep flows? Or to real flows observed in the laboratory, rather than simulated in primitive-equation models? The existing literature sheds little light on the answers to these questions.

The current paper aims to test the limits of quasi-geostrophic theory by systematically comparing its predictions with laboratory observations of flows that are deep, have moderate Rossby number and contain ubiquitous ageostrophic inertia–gravity waves. We describe the laboratory annulus in § 2 and the numerical quasi-geostrophic model in § 3. We compare equilibrated baroclinic wave flows in the laboratory and in the model in § 4, considering wavenumber regime diagrams (§ 4.1), wave amplitudes (§ 4.2) and wave speeds (§ 4.3). In each case, we propose and test physical mechanisms responsible for the model's biases compared with the laboratory. We conclude with a summary and discussion in § 5.

2. Description of the laboratory experiment

The laboratory apparatus we employ is shown in figure 1 and has been used by King (1979), Appleby (1982), Lovegrove (1997) and Williams (2003). The annular tank has inner radius $L = 62.5\,\mathrm{mm}$, outer radius $2L = 125.0\,\mathrm{mm}$ and depth $2H = 250.0\,\mathrm{mm}$. The tank contains two immiscible liquids with equal resting depths of $H = 125.0\,\mathrm{mm}$. The tank is mounted on a circular turntable that rotates with angular velocity $\Omega \geqslant 0$. The tank's lid, which is in contact with the upper liquid, rotates with angular velocity $\Delta\Omega \geqslant 0$ relative to the tank, in order to drive a velocity shear across the internal interface and induce baroclinic instability. The upper layer is water, of density $\rho_1 = 997\,\mathrm{kg\,m^{-3}}$ and kinematic viscosity $\nu_1 = 1.27 \times 10^{-6}\,\mathrm{m^2\,s^{-1}}$, and the lower layer is a limonene–chlorofluorocarbon mixture, of composite density $\rho_2 = 1003\,\mathrm{kg\,m^{-3}}$ and kinematic viscosity $\nu_2 = 1.08 \times 10^{-6}\,\mathrm{m^2\,s^{-1}}$. The surface tension at the internal interface is $S = 29.0 \times 10^{-3}\,\mathrm{N\,m^{-1}}$. The acceleration due to gravity is $g = 9.81\,\mathrm{m\,s^{-2}}$.

To visualize the height of the internal interface, white light from a lamp on the laboratory floor passes upwards through the base, liquids and lid, which are all transparent. The light is received by a colour video camera that is mounted near the ceiling on a frame attached to the turntable. Different interface heights cause different colours to be registered by the camera because limonene is optically active

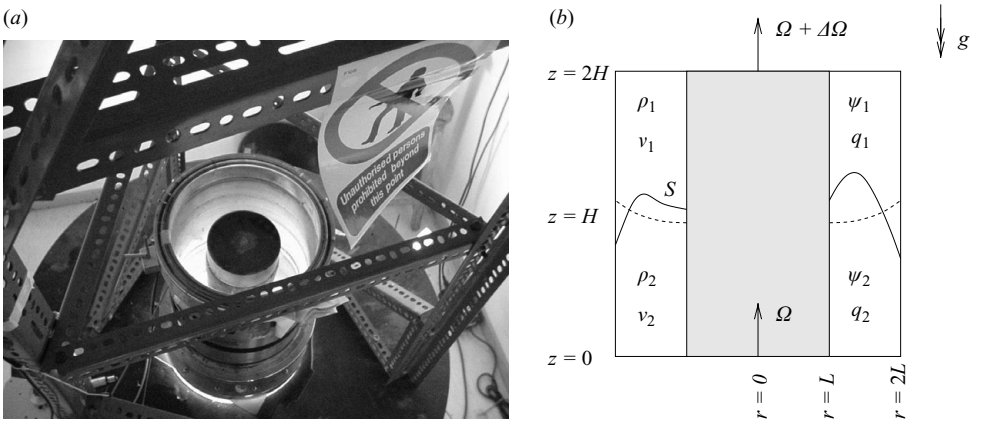

FIGURE 1. (*a*) Photograph of the laboratory apparatus from above, showing the circular turntable, annular tank and mounted frame. (*b*) Schematic vertical cross-section through the annulus. The dashed line shows a possible resting parabolic interface height (attained when $\Delta\Omega = 0$), and the solid line shows a possible perturbed interface height (attained when $\Delta\Omega \neq 0$). See the text for definitions of variables.

and the annulus is viewed through crossed polaroids, following Hart & Kittelman (1986). Williams, Read & Haine (2004*b*) have calibrated the experiment, by deriving the quantitative relationship between interface height and colour.

The control parameters are Ω and $\Delta\Omega$, from which we construct a two-dimensional parameter space spanned by the internal rotational Froude number (F) and the dissipation parameter (d), which are dimensionless quantities defined by

$$F = \frac{f^2 L^2}{g' H} \tag{2.1}$$

and

$$d = \frac{\sqrt{\overline{\nu}\Omega}}{H\Delta\Omega}\ , \tag{2.2}$$

where $f = 2\Omega$ is the Coriolis parameter; $g' = 2g(\rho_2 - \rho_1)/(\rho_1 + \rho_2)$ is the reduced gravity; and $\overline{\nu} = (\nu_1 + \nu_2)/2$ is the mean kinematic viscosity.

The laboratory experiments lie well outside the formal quasi-geostrophic regime, for three independent reasons. First, in the regular baroclinic wave regime of interest in the current paper, the bulk Rossby number ($\Delta\Omega/2\Omega$) reaches values as large as 1 (see figure 3 of Williams *et al.* 2005). Second, the depth-to-width aspect ratio ($2H/L = 4$) is large. Third, the fluid contains ubiquitous ageostrophic inertia–gravity waves (Williams, Haine & Read 2008), which are relatively weak but which nevertheless contribute to departures from geostrophic balance. Therefore, quasi-geostrophic theory – an asymptotic approximation to the shallow-water equations for small Rossby numbers – is formally inapplicable.

Before proceeding, we briefly qualify our above remark that the presence of ageostrophic inertia–gravity waves is inconsistent with quasi-geostrophic theory. Certainly, quasi-geostrophic theory cannot capture the inertia–gravity waves. But their presence does not necessarily limit the applicability of quasi-geostrophic theory to the larger scales of motion if the inertia–gravity waves interact negligibly with those scales. Indeed, for small Rossby numbers, non-interaction theorems (e.g. Greenspan 1968) limit the ability of the inertia–gravity waves to interact with the large-scale

flow. However, for $O(1)$ Rossby numbers, such as those encountered in the present experiments, the non-interaction theorems fail to hold, and the ability of quasi-geostrophic theory to describe the large-scale flow may be compromised.

3. Description of the quasi-geostrophic model

Previous studies have employed rectangular channel geometry to approximately model the cylindrical annulus (e.g. Brugge *et al.* 1987). Rectangular channel geometry with periodic along-channel boundary conditions is a good approximation to cylindrical annulus geometry only if the width of the annulus is much smaller than the mean radius (King 1979). However, the ratio of the former to the latter in the present annulus is 2/3, which is not much smaller than unity. Furthermore, the periodic rectangular channel has additional shift–reflect symmetries that are absent in the annulus (Cattaneo & Hart 1990). As a result, certain wave–wave interaction coefficients vanish in the channel but not in the annulus (Kwon & Mak 1988). Therefore, for the present numerical simulations, we choose a bespoke annulus model that fully retains the effects of cylindrical geometry. The model is the QUAsi-Geostrophic Model for Investigating Rotating fluids Experiments (QUAGMIRE). This section will summarize the salient features of QUAGMIRE. A comprehensive technical description is given by Williams *et al.* (2009).

Referring to figure 1(*b*), the model employs cylindrical polar coordinates (r, θ, z) fixed in the turntable frame. The stream functions are $\psi_i(r, \theta, t)$, and the quasi-geostrophic potential vorticities are $q_i(r, \theta, t)/H$, where $i = 1$ refers to the upper layer and $i = 2$ refers to the lower layer. The (dimensional) equations governing the evolution of quasi-geostrophic motions, integrated by QUAGMIRE, are

$$\frac{\partial q_1}{\partial t} = \frac{1}{r}\frac{\partial \psi_1}{\partial \theta}\frac{\partial q_1}{\partial r} - \frac{1}{r}\frac{\partial \psi_1}{\partial r}\frac{\partial q_1}{\partial \theta} - \frac{\sqrt{\Omega \nu_1}}{H}\left[\nabla^2\psi_1 + \chi_2\nabla^2(\psi_1 - \psi_2)\right] + \frac{2\Delta\Omega\sqrt{\Omega\nu_1}}{H}, \quad (3.1)$$

$$\frac{\partial q_2}{\partial t} = \frac{1}{r}\frac{\partial \psi_2}{\partial \theta}\frac{\partial q_2}{\partial r} - \frac{1}{r}\frac{\partial \psi_2}{\partial r}\frac{\partial q_2}{\partial \theta} - \frac{\sqrt{\Omega \nu_2}}{H}\left[\nabla^2\psi_2 + \chi_1\nabla^2(\psi_2 - \psi_1)\right], \quad (3.2)$$

where

$$q_1 = \nabla^2\psi_1 + \frac{f^2}{g'H}(\psi_2 - \psi_1) + \frac{f}{H}\frac{r^2\Omega^2}{2g}, \quad (3.3)$$

$$q_2 = \nabla^2\psi_2 - \frac{f^2}{g'H}(\psi_2 - \psi_1) - \frac{f}{H}\frac{r^2\Omega^2}{2g} \quad (3.4)$$

and $\chi_i = \sqrt{\nu_i}/(\sqrt{\nu_1} + \sqrt{\nu_2})$.

In (3.1) and (3.2), the nonlinear Jacobian terms represent advection of potential vorticity by the geostrophic flow; the Laplacian terms represent parameterized dissipation of potential vorticity by the thin Ekman (1905) layers at the lid ($\nabla^2\psi_1$), base ($\nabla^2\psi_2$) and interface ($\pm\nabla^2(\psi_1 - \psi_2)$); and the constant term in (3.1) represents parameterized generation of potential vorticity by the differentially rotating lid, communicated to the fluid by the Ekman layer. In (3.3) and (3.4), the first terms on the right represent the contribution to the potential vorticity from vortices within the layers; the middle terms represent the contribution from vortex stretching and compression because of interface perturbations; and the final terms represent the contribution from the basic centrifugal parabolic interface deflection (the quadratic β-effect; e.g. Bouchet & Sommeria 2002). The effects of interfacial surface tension are neglected (but see § 4.2). The equilibrium solution to (3.1)–(3.4) consists of solid-body rotation at rate $\Delta\Omega(2 + \chi)/[2(1 + \chi)]$ in the upper layer and $\Delta\Omega/[2(1 + \chi)]$ in

the lower layer, where $\chi = \sqrt{\nu_2/\nu_1}$ (Hart 1972). For certain parameter values, weak perturbations to this equilibrium solution may grow because of baroclinic instability and equilibrate at finite amplitude.

Inversion of the elliptic equations (3.3) and (3.4), to obtain ψ_1 and ψ_2 from q_1 and q_2 at each time step, is achieved in QUAGMIRE by first projecting on to the vertical and azimuthal normal modes of those equations and then, for each mode, solving a second-order ordinary differential equation for the radial structure. The flow in the laboratory annulus satisfies the impermeability condition and the no-slip condition at both lateral boundaries, yielding four boundary conditions. But the radial structure equation contains only second-order radial derivatives, and so only two of the four boundary conditions may be applied. Therefore, we are forced to use a reduced set of boundary conditions.

The over-constrained nature of the potential vorticity inversion in quasi-geostrophic models has been discussed by Williams (1979). Physically, the problem occurs because (3.3) and (3.4) contain no lateral viscosity terms and cannot capture the thin viscous Stewartson (1957) layers at the lateral boundaries. The inclusion of lateral viscosity terms, through the addition of $\nu_1\nabla^4\psi_1$ to (3.1) and $\nu_2\nabla^4\psi_2$ to (3.2), following McWilliams (1977) and Flierl (1977), would allow the Stewartson layers to be captured. But the no-slip condition could then be imposed only by artificially modifying the boundary values of the stream functions, obtained through inversion of (3.3) and (3.4) subject to impermeability, before using them in the laterally viscous extensions to (3.1) and (3.2). We reject this approach because the stream functions and potential vorticities used in (3.1) and (3.2) would then be inconsistent, i.e. would not satisfy (3.3) and (3.4).

How to choose appropriate lateral boundary conditions in laterally inviscid quasi-geostrophic models has long been debated. Perturbations to the equilibrium solid-body rotation flow may be decomposed into azimuthal waves and a correction to the azimuthal-mean flow. Phillips (1954, 1956) imposed impermeability on the waves and the no-slip condition on the mean-flow correction (which satisfies impermeability by construction). But the latter condition was abandoned by Phillips (1963) and Pedlosky (1964), leading to a spurious non-physical energy flux through the lateral boundaries (McIntyre 1967). Again, the condition was imposed by Pedlosky (1970) but later abandoned (Pedlosky 1971, 1972), on the grounds of being 'the only apparently feasible way of making progress' with the analytical solution. Pedlosky's calculations have since been repeated with the condition imposed (Smith 1974, 1977; Smith & Pedlosky 1975).

We presently avoid the spurious energy flux by imposing the full original boundary conditions of Phillips (1954, 1956) in the QUAGMIRE model. The no-slip condition is imposed on the mean-flow correction during the elliptic potential vorticity inversion. We stress that the no-slip condition is imposed, not to capture the Stewartson (1957) boundary layers, which are fundamentally viscous, but rather to suppress the spurious energy source that is otherwise present. Lateral viscosity, whether molecular or turbulent or numerical, is not needed to do this.

For the present numerical integrations of (3.1)–(3.4) using QUAGMIRE, as for previous integrations (e.g. Williams, Haine & Read 2004*a*), ψ_i and q_i are co-located on a regular grid composed of 16 points in the radial direction (including one point on each lateral boundary) and 96 points in the azimuthal direction. This choice yields grid boxes near the inner boundary that are approximately square and of side length 4 mm. For comparison, the baroclinic deformation radius is around 15 mm. The leapfrog time-stepping scheme is used, including a Robert (1966) time filter (with

parameter 0.01) to suppress the computational mode (Mesinger & Arakawa 1976). The time step Δt is chosen such that the bulk azimuthal Courant number $\Delta\Omega\,\Delta t/2\Delta\theta$ is 0.01. The Arakawa (1966) discretization of the Jacobian and the standard five-point discretization of the Laplacian are used.

Very weak diffusion of potential vorticity, of the form $\nabla^2 q_i$, is added to the right sides of (3.1) and (3.2), as is usual in numerical models (e.g. Lewis 1992). We stress that this is done not to capture the Stewartson (1957) boundary layers but rather to avoid a non-physical build-up of energy near the grid scale. The diffusion coefficient is chosen such that the e-folding time for the damping of mid-radius grid-scale features is equal to one lid rotation period; a typical numerical value is $10^{-7}\,\mathrm{m^2\,s^{-1}}$. All the diffusion terms are time-lagged by one time step to avoid the well-known computational instability (Haltiner & Williams 1980).

Williams *et al.* (2009) have demonstrated numerical convergence for the parameter values given above, by showing that simulations are insensitive to changes in the grid spacing, potential vorticity diffusion coefficient and Robert parameter.

4. Comparison between laboratory experiment and quasi-geostrophic model

Mindful that the laboratory experiments lie outside the quasi-geostrophic regime, we wish to determine the extent to which the fluid dynamics of equilibrated baroclinic waves are captured by the quasi-geostrophic equations (3.1)–(3.4). To this end, laboratory data are obtained from a series of experiments, each with $\Delta\Omega$ held constant at a value below $3.1\,\mathrm{rad\,s^{-1}}$ and with Ω slowly increasing from 0 to $4.3\,\mathrm{rad\,s^{-1}}$ over 3 h. We compare the laboratory observations with 210 QUAGMIRE simulations, one for each combination of $\Omega/\mathrm{rad\,s^{-1}} \in \{1.00, 1.50, 1.75, 2.00, 2.25, 2.50, 2.75, 3.00, 3.25, 3.50\}$ and $\Delta\Omega/\mathrm{rad\,s^{-1}} \in \{0.01, 0.02, 0.03, 0.04, 0.05, 0.06, 0.08, 0.10, 0.12, 0.15, 0.20, 0.23, 0.30, 0.40, 0.50, 0.60, 0.70, 0.85, 1.06, 1.31, 1.61\}$, giving a roughly uniform density of sampled points in the $(\log[d], F)$ parameter space. Each model integration is initiated from the equilibrium solid-body rotation flow plus a very weak random perturbation to seed any baroclinic instability and is continued until long after any baroclinic wave has equilibrated.

The following sections compare wavenumber regime diagrams (§ 4.1), wave amplitudes (§ 4.2) and wave speeds (§ 4.3) between the laboratory and the model.

4.1. *Wavenumber regime diagrams*

We categorize flows in the laboratory and model according to the dominant azimuthal wavenumber of the equilibrated baroclinic wave, which is always found to be 1, 2 or 3 within the parameter ranges explored herein. In the absence of baroclinic instability, baroclinic waves do not form and the flow remains axisymmetric. Figure 2 compares the resulting wavenumber regime diagrams. The non-trivial topology of the laboratory bifurcation structure, which is a consequence of wave competition, is convincingly captured by the model. There is excellent qualitative agreement between the shapes of the regime transition curves. In the limit of zero dissipation parameter, the Phillips (1954) model of baroclinic instability predicts a critical Froude number of $\pi^2/2 \approx 4.9$ for the neutral curve, in good agreement with both regime diagrams. The increase of the critical Froude number with increasing dissipation parameter, seen in both regime diagrams, is captured by the dissipative extension to the Phillips model (e.g. § 7.12 of Pedlosky 1987).

Many quantitative aspects of the comparison between the two regime diagrams are convincing, such as the relative sizes of the three wavenumber regimes. The

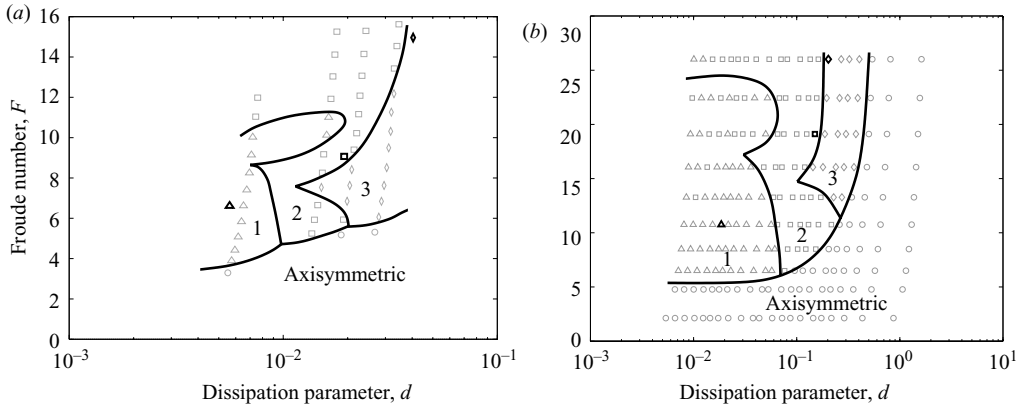

FIGURE 2. Azimuthal wavenumber regime diagrams from (*a*) the laboratory and (*b*) the model. The symbols categorize the dominant flow at each measurement point: the circles denote axisymmetric flow; the triangles denote wave 1 flow; the squares denote wave 2 flow; and the diamonds denote wave 3 flow. The sampling is much sparser in the laboratory than in the model. Regime transition curves are inferred and over-plotted. In (*a*), which is adapted from figure 7 of Lovegrove, Read & Richards (2000), the three bold symbols indicate the parameter locations of figure 3 (*a*, *c*, *e*). In (*b*), the three bold symbols indicate the parameter locations of figure 3 (*b*, *d*, *f*). The model wave 1 and wave 2 regimes become entangled at low d and high F because of extreme initial condition sensitivity. Note the different axis limits in (*a*) and (*b*).

quantitative agreement is not wholly satisfactory, however. The (d, F) coordinates of the axisymmetric/wave 1/wave 2 triple point are (0.01, 4.6) in the laboratory and (0.07, 6.1) in the model, and those of the axisymmetric/wave 2/wave 3 triple point are (0.02, 5.6) in the laboratory and (0.3, 11) in the model. Therefore, the model overestimates F by a factor of around 1–2 and d by a factor of around 5–10. This bias appears to be robust in quasi-geostrophic models. For example, in a quasi-geostrophic spectral channel model of the annulus, Lovegrove (1997) found that 'while the Froude numbers of experimental runs are of the same magnitude as those present in the theoretical regime diagram, the experimental values of the dissipation parameter are actually about an order of magnitude smaller than the predicted theoretical values'. The dissipation parameter is a non-dimensional measure of the magnitude of the Ekman-layer terms in (3.1) and (3.2). Therefore, we infer that the assumption of linear parameterized Ekman-layer pumping and suction velocities, used here and by Lovegrove (1997), is inadequate if quantitative agreement is sought.

It might reasonably be wondered whether much advantage derives from the nonlinear component of the model and whether linear quasi-geostrophic theory is all that is needed to capture the bifurcation structure observed in the laboratory. Lovegrove (1997) derived neutral curves from linear quasi-geostrophic theory and plotted a regime diagram (figure 5.11 therein). The correspondence with our regime diagram, derived from nonlinear quasi-geostrophic theory (figure 2*b*), is mixed. The ax $\leftrightarrow$ 1, ax $\leftrightarrow$ 2 and ax $\leftrightarrow$ 3 transition curves are captured well, but the 1 $\leftrightarrow$ 2 and 2 $\leftrightarrow$ 3 transition curves are not. Evidently, nonlinear effects are important for wavenumber selection when two or more unstable wave modes compete. Indeed, many authors (e.g. Hart 1981; Pedlosky 1981; Appleby 1982) have demonstrated that the selected wave, in a flow that is simultaneously baroclinically unstable to more than one wave mode, is not necessarily the one with the largest linear growth rate. We conclude that linear quasi-geostrophic theory is not sufficient to reproduce all

the regime boundaries seen in the laboratory (figure 2*a*). Only the nonlinear quasi-geostrophic model can fully reproduce the bifurcation structure. Of course, nonlinear effects are also important for determining the equilibrated wave amplitudes, because waves growing from baroclinic instability would grow exponentially and indefinitely in a linear quasi-geostrophic model.

4.2. *Wave amplitudes*

A systematic comparison of equilibrated wave amplitudes is difficult because a given Ω and $\Delta\Omega$ (or d and F) generally correspond to different wavenumber regimes in the laboratory and the model. Instead, we choose approximately corresponding wave 1, wave 2 and wave 3 case-study flows by visual inspection of figure 2. The basic interface height structures of the three case-study flows are compared in figure 3. The laboratory and model waves are qualitatively very similar.

The interface height waves are compared quantitatively in figure 4, after projecting the laboratory waves on to the calibration curve derived by Williams *et al.* (2004*b*). Curiously, the laboratory curves are seen to contain substantial admixtures of modes other than the dominant mode, but the model curves are much more monochromatic. For the wave 1, wave 2 and wave 3 flows, respectively, the mid-radius amplitudes are around 25, 8 and 7 mm in the laboratory and 4, 2 and 1 mm in the model. Therefore, although the model correctly captures the decreasing amplitude with increasing wavenumber observed in the laboratory, the model waves are a few times weaker than the laboratory waves. The laboratory and model structures clearly correlate very well by visual inspection, however, and only really differ in amplitude, not pattern. Note that although there is a well-known correction to the Ekman pumping velocity at finite Rossby numbers (e.g. Hart 1995), which scales linearly with the Rossby number and which could in principle modify the amplitude of the equilibrated waves, our observed wave amplitude bias persists even at small Rossby numbers and so evidently cannot be explained by this mechanism.

We propose that the wave amplitude bias is caused by the model's neglect of surface tension effects at the interface between the two liquids. The non-dimensional parameter describing the relative importance of these effects is the product of the Froude number and the interfacial tension number (Appleby 1982; Williams *et al.* 2009), where the latter is defined by

$$I = \frac{S}{g(\rho_2 - \rho_1)L^2} \,. \tag{4.1}$$

In the present laboratory setting, we have $I = 0.13$. Therefore, the product FI may exceed unity if the Froude number is large. We conclude that interfacial surface tension effects may be non-negligible and that the quasi-geostrophic model may benefit from their inclusion. In the limit of weak interfacial surface tension, i.e. $FI \ll 1$, analytical progress is possible. In this limit, Williams *et al.* (2009) have shown that (3.1) and (3.2) are unmodified but that (3.3) and (3.4) become

$$q_1 = \nabla^2\psi_1 + \frac{f^2}{g'H}\left(1 + \frac{S}{g(\rho_2 - \rho_1)}\nabla^2\right)(\psi_2 - \psi_1) + \frac{f}{H}\frac{r^2\Omega^2}{2g} \,, \tag{4.2}$$

$$q_2 = \nabla^2\psi_2 - \frac{f^2}{g'H}\left(1 + \frac{S}{g(\rho_2 - \rho_1)}\nabla^2\right)(\psi_2 - \psi_1) - \frac{f}{H}\frac{r^2\Omega^2}{2g} \,. \tag{4.3}$$

The new terms, involving the operator $[S/g(\rho_2 - \rho_1)]\nabla^2$, describe the leading-order effects of weak interfacial surface tension and are comparatively small in the limit under consideration. The physics encapsulated in the new terms is that interfacial

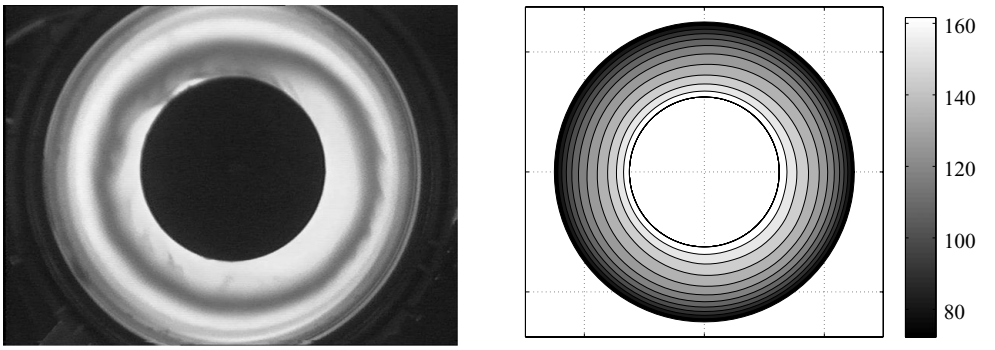

(a) $\Omega = 1.76$ rad s^{-1}, $\Delta\Omega = 2.03$ rad s^{-1} (d, F) = (0.0057, 6.6)

(b) $\Omega = 2.25$ rad s^{-1}, $\Delta\Omega = 0.70$ rad s^{-1} (d, F) = (0.019, 10.8)

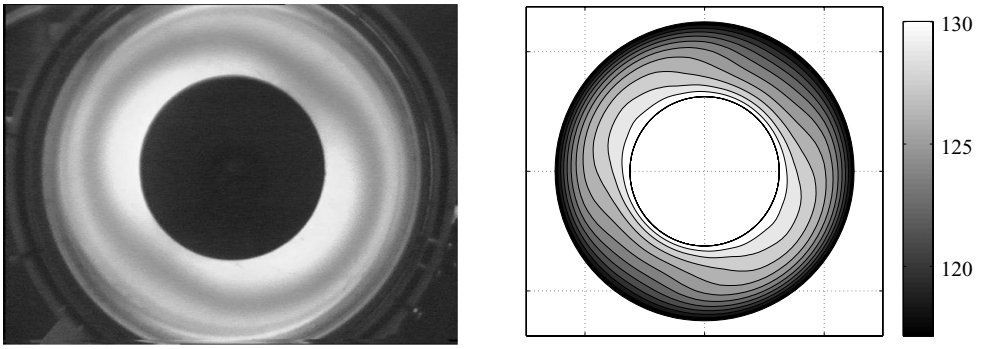

(c) $\Omega = 2.03$ rad s^{-1}, $\Delta\Omega = 0.62$ rad s^{-1} (d, F) = (0.020, 8.8)

(d) $\Omega = 3.00$ rad s^{-1}, $\Delta\Omega = 0.10$ rad s^{-1} (d, F) = (0.15, 19.1)

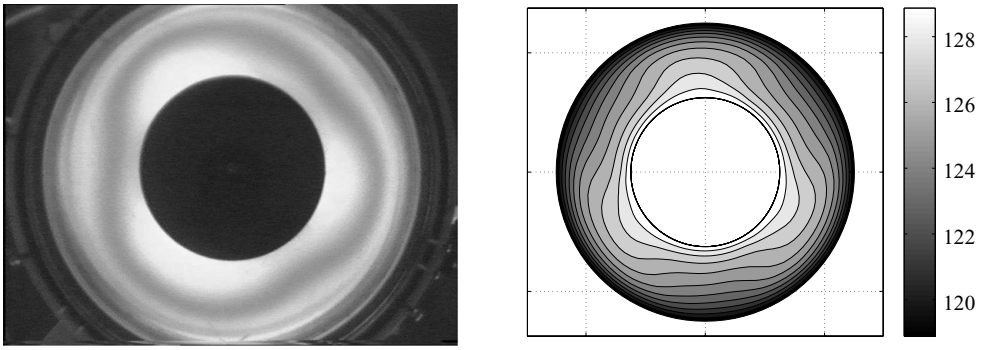

(e) $\Omega = 2.66$ rad s^{-1}, $\Delta\Omega = 0.35$ rad s^{-1} (d, F) = (0.040, 15.0)

(f) $\Omega = 3.50$ rad s^{-1}, $\Delta\Omega = 0.08$ rad s^{-1} (d, F) = (0.20, 26.0)

FIGURE 3. Maps of equilibrated interface height from the laboratory (left column) and the model (right column) for wave 1 flows (top row), wave 2 flows (middle row) and wave 3 flows (bottom row). The corresponding parameters are given below each plot, and their locations within the (d, F) parameter space are indicated in figure 2. In the laboratory plots, which are greyscale versions of colour images recorded by the video camera, there is a many-to-one mapping from interface height to light intensity. In the model plots, the unit used is the millimetre. The azimuthal orientations of the waves are arbitrary.

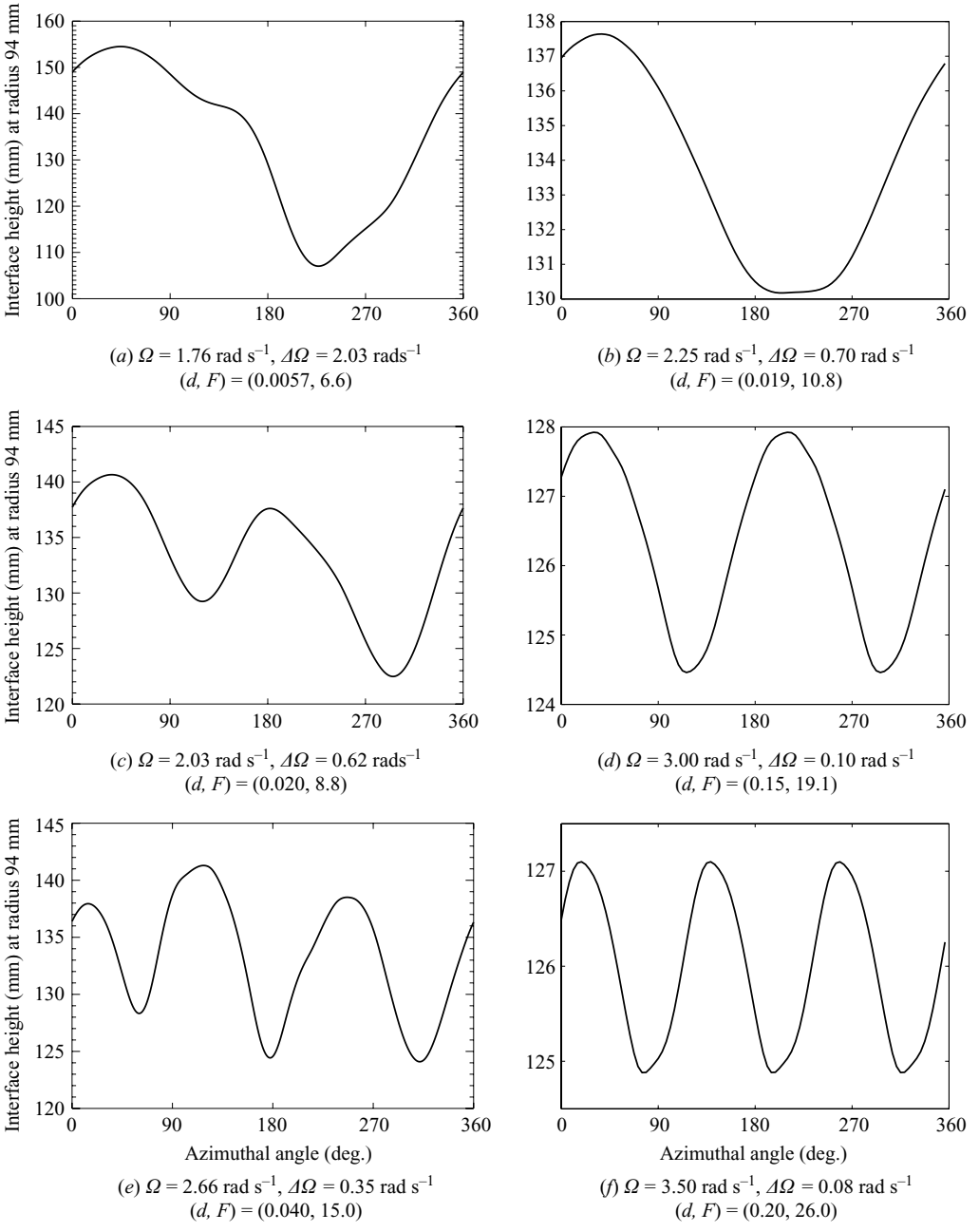

FIGURE 4. Profiles of equilibrated interface height in the middle of the annular gap (i.e. at $r = 94$ mm) in the maps of figure 3, from the laboratory (left column) and the model (right column) for wave 1 flows (top row), wave 2 flows (middle row) and wave 3 flows (bottom row). The corresponding parameters are given below each plot. The azimuthal orientations of the waves are arbitrary. Referring to figure 3, the zero of azimuth is at '3 o'clock', and azimuth increases in the clockwise direction. Note the different ordinate scales between the laboratory and model plots.

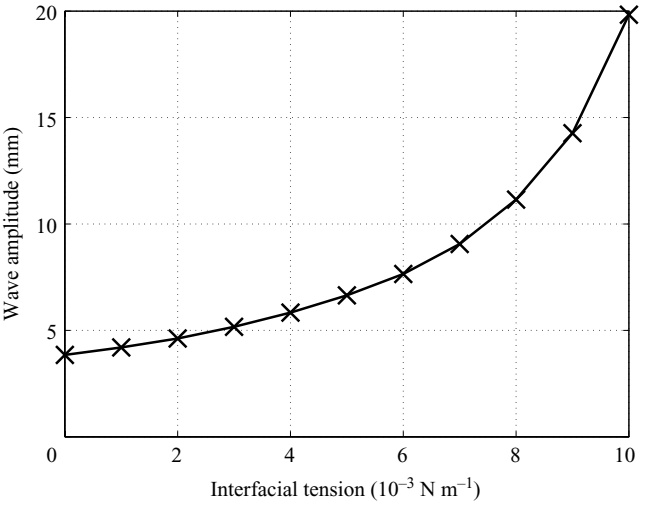

FIGURE 5. Equilibrated mid-radius wave amplitude in the quasi-geostrophic model, plotted against interfacial surface tension, for a wave 1 flow with $\Omega = 2.25\,\mathrm{rad\,s^{-1}}$ and $\Delta\Omega = 0.60\,\mathrm{rad\,s^{-1}}$.

surface tension strengthens the horizontal gradient of the hydrostatic pressure difference between the lid and the base, intensifying the geostrophic velocity shear across the internal interface and increasing the baroclinicity of the fluid. Therefore, we expect interfacial surface tension to increase the amplitude of baroclinic waves.

To substantiate our proposed mechanism for the model's wave amplitude bias, we perform additional QUAGMIRE integrations with (4.2) and (4.3) replacing (3.3) and (3.4). In a case-study wave 1 simulation, we increase S from 0 to $10.0 \times 10^{-3}\,\mathrm{N\,m^{-1}}$ in 10 discrete steps, allowing the flow to equilibrate fully after each increase. The corresponding value of the product FI increases from 0 to 0.47. The equilibrated state remains a wave 1 flow throughout, and the basic flow pattern is unmodified. But, as shown in figure 5, the amplitude of the equilibrated wave increases by a factor of around 5 as the interfacial surface tension is increased. Similar results are found for other wavenumbers. We cannot further increase S to match the value of $29.0 \times 10^{-3}\,\mathrm{N\,m^{-1}}$ measured in the laboratory, because the product FI becomes too large for the representation embodied in (4.2) and (4.3) to be valid. Nevertheless, we are persuaded that the wave amplitude bias in the original model integrations can probably be accounted for by their neglect of interfacial surface tension.

Finally, we repeat a subset of the original 210 QUAGMIRE integrations, with (4.2) and (4.3) replacing (3.3) and (3.4) and using a nominal value of $5.0 \times 10^{-3}\,\mathrm{N\,m^{-1}}$ for the interfacial surface tension. The subset is that for which $FI < 0.3$ (i.e. $F < 13$), which is the largest value for which the assumption $FI \ll 1$ could reasonably be expected to apply. The resulting regime diagram (not shown) closely matches the original one (figure 2*b*). We conclude that weak interfacial surface tension does not affect the regime diagram but substantially increases the wave amplitudes.

4.3. *Wave speeds*

Returning to the original set of surface-tension-free QUAGMIRE integrations, figure 6 shows the dependence of the phase speed of the baroclinic wave on the differential lid rotation rate, for fixed turntable rotation rate. The wave speed is proportional to the lid rotation rate in both the laboratory and the model. The

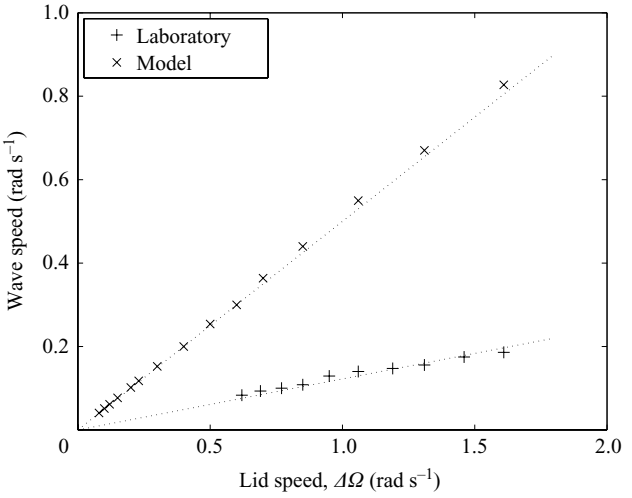

FIGURE 6. Angular azimuthal phase speed of equilibrated baroclinic waves, in the laboratory experiment and the quasi-geostrophic model, plotted against $\Delta\Omega$ for the case $\Omega = 2.0\,\mathrm{rad\,s^{-1}}$. Similar results are found at other values of Ω. Also shown are straight dotted lines of gradients 0.50 and 0.12 passing through the origin.

proportionality constants differ, however. The wave speed (in the turntable frame) is equal to $0.12\Delta\Omega$ in the laboratory and $0.50\Delta\Omega$ in the model. Therefore, the model overestimates the wave speeds by a factor of around 4. These results are unmodified by the inclusion of weak interfacial surface tension, as implemented in § 4.2.

We propose that the phase speed bias is caused by the model's neglect of Stewartson-layer drag at the lateral boundaries. As discussed in § 3, the potential vorticity inversion in quasi-geostrophic models is over-constrained. Either the impermeability condition or the no-slip condition, but not both, may be imposed on the waves at the lateral boundaries. Since impermeability is the more basic requirement, the no-slip condition is abandoned, and the Stewartson layers are necessarily neglected as a consequence. We note that the nonlinear evolution of baroclinic waves in a two-layer channel is known to be sensitive to the lateral boundary conditions for typical laboratory parameter values (e.g. Mundt, Brummell & Hart 1995*a*).

To substantiate our proposed mechanism for the model's wave speed bias, we apply torque-balance considerations to calculate and compare the equilibrium flow in the annulus, both with and without Stewartson layers. The two inviscid interiors are modelled as rotating solid bodies, acted upon by torques due to velocity shears across the Ekman boundary layers at the lid, base and internal interface and across the Stewartson boundary layers at the sidewalls. In equilibrium, the net torque acting on each inviscid interior must be zero, yielding two coupled nonlinear algebraic equations for the solid-body rotation rates in the upper and lower layers. Williams *et al.* (2004*b*) have derived the equations and described a convergent iterative method for obtaining solutions.

We apply the torque-balance analysis to case-study flows with $\Omega = 2.0\,\mathrm{rad\,s^{-1}}$ and various values of $\Delta\Omega$. For these flows, the Ekman-layer depth $(\overline{\nu}/\Omega)^{1/2}$ is 0.8 mm and the Stewartson-layer width $(\overline{\nu}L^2/\Omega)^{1/4}$ is 7.0 mm. The results of the calculations are shown in figure 7. As expected, the solid-body rotation rates in the upper and lower layers are substantially reduced when Stewartson-layer drag is included in the torque balance, compared with when it is neglected. Taking an average over the upper and

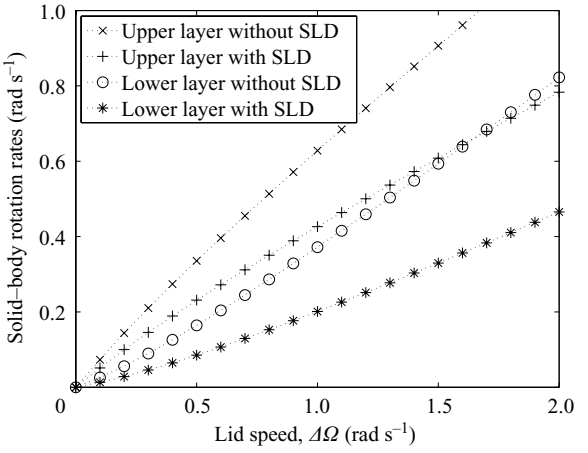

FIGURE 7. Equilibrium solid-body rotation rates in the upper and lower layers, both with and without Stewartson-layer drag (SLD), plotted against $\Delta\Omega$ for the case $\Omega = 2.0\,\mathrm{rad\,s^{-1}}$. The data are obtained from a torque-balance calculation described in the text. Similar results are found at other values of Ω.

lower layers yields rotation rates for the vertically averaged flow. When Stewartson-layer drag is neglected, the vertically averaged flow rotates at $0.50\Delta\Omega$, in agreement with the baroclinic wave speed of $0.50\Delta\Omega$ seen in the quasi-geostrophic model. But when Stewartson-layer drag is included, the vertically averaged flow rotates at only $0.31\Delta\Omega$, for comparison with the baroclinic wave speed of $0.12\Delta\Omega$ measured in the laboratory.

Two caveats apply when comparing the predictions of the torque-balance analysis with the baroclinic wave speeds. First, the torque-balance analysis applies only to the axisymmetric equilibrium flow and hence neglects the contributions of the baroclinic waves to the Ekman-layer torques at the internal interface (which presumably increase the drag). Second, baroclinic waves are not necessarily expected to travel at the same speed as the vertically averaged flow. Indeed, measurements in the laboratory annulus have revealed that baroclinic waves travel substantially slower than the vertically averaged flow (Lovegrove 1997). Therefore, despite the large apparent discrepancy between $0.31\Delta\Omega$ and $0.12\Delta\Omega$, we are persuaded that (at least the majority of) the wave speed bias in the quasi-geostrophic model can be accounted for by the neglect of Stewartson-layer drag at the lateral boundaries.

5. Summary and discussion

We have compared laboratory observations of equilibrated baroclinic waves in the rotating two-layer annulus with numerical simulations from a bespoke quasi-geostrophic model named QUAGMIRE. The laboratory experiments lie well outside the quasi-geostrophic regime: the Rossby number reaches unity; the depth-to-width aspect ratio is large; and the fluid contains ageostrophic inertia–gravity waves. The comparison was motivated by a desire to test the ability of quasi-geostrophic theory to adequately describe the fluid dynamics of such non-quasi-geostrophic flows.

Qualitatively, the quasi-geostrophic model captures many aspects of the laboratory flows remarkably well, despite being formally inapplicable. The laboratory and the model both exhibit a curve of marginal baroclinic instability in the (d, F)-plane. On the high-F side of the curve, baroclinic waves of wavenumber 1, 2 and 3 develop,

and on the low-F side, the flow remains axisymmetric. The non-trivial topology of the wavenumber bifurcation structure in the laboratory is convincingly captured by the model. The observed decrease of baroclinic wave amplitude with increasing wavenumber and the observed proportionality between baroclinic wave speed and lid rotation rate are also convincingly captured.

Quantitatively, the model displays three systematic biases compared with the laboratory. First, in a comparison of the parameter locations of the wavenumber bifurcation structures, the model and laboratory Froude numbers agree to within a factor of 2, but the dissipation parameters differ by an order of magnitude. Second, the interfacial amplitudes of baroclinic waves in the model are a few times smaller than those measured in the laboratory. Third, baroclinic waves in the model propagate around four times faster than those in the laboratory.

We have presented evidence that the model's biases are consequences of its treatment of boundary layers (both Ekman and Stewartson) and neglect of interfacial surface tension. Therefore, the biases can probably be explained without invoking the dynamical effects of the moderate Rossby number, large aspect ratio or inertia–gravity waves. Quasi-geostrophic dynamics, with a more faithful treatment of the boundary layers and surface tension, could probably accurately describe the laboratory flow, despite the flow lying well outside the quasi-geostrophic regime.

Despite the model's quantitative shortcomings, the non-trivial wavenumber bifurcation structure in the (d, F)-plane is convincingly captured. We consider this to be a stringent test of the model's fidelity. The implication is that the bifurcation structure is insensitive to the model's biases in wave amplitudes and speeds, the large aspect ratio, the moderate Rossby number, the presence of inertia–gravity waves in the laboratory, the greater degree of modal monochromaticity seen in the model compared with the laboratory, the model's neglect of interfacial surface tension and the model's treatment of Ekman and Stewartson layers. This is an unexpected and intriguing result that could not have been predicted from the existing literature. It is also potentially useful, for example by permitting the use of a low-order quasi-geostrophic model to easily map out the bifurcation structure – which would be very difficult with a primitive equations model – followed by the use of a primitive equations model for more quantitative agreement in specific cases.

It would be interesting to extend our comparison to more turbulent flow regimes. For the experiments presented herein, the bulk Reynolds number of the annulus $Re = L^2 \Delta\Omega / \overline{\nu}$, based on the molecular viscosity, typically ranges from 30 to 5000. In contrast, the Reynolds number typically reaches 10^6 or 10^7 in the atmosphere and 10^8 or 10^9 in the oceans (Read 2001). Unfortunately, we cannot access the high-Re turbulent regime with the present apparatus. For example, to achieve $Re = 10^8$ using liquids of molecular viscosity $\overline{\nu} = 1.2 \times 10^{-6}\,\mathrm{m^2 s^{-1}}$ in an annulus of width $L = 62.5\,\mathrm{mm}$, we would need to differentially rotate the lid at $\Delta\Omega = 30\,000\,\mathrm{rad\,s^{-1}}$, which well exceeds the maximum permissible rotation rate. Although we could easily explore this regime in the model, there seems little point if the corresponding laboratory data are unavailable for comparison. Therefore, we leave questions about the applicability of quasi-geostrophic theory in the turbulent regime as future work for a group with a larger annulus (e.g. the rotating tank with a diameter of 14 m at the Laboratoire des Ecoulements Géophysiques et Industriels in Grenoble) or less viscous working liquids.

Furthermore, it would be interesting to compare, between the laboratory experiment and the numerical model, the basic solid-body rotation fields used for the stability analysis. This is because each Stewartson layer occupies around 10 % of the radial

domain. The Stewartson layers will inevitably affect the structure of the mean flow, which could in turn affect the wave amplitudes and phase speeds and could considerably alter the nature of the instability. Indeed, the presence of horizontal shear in the Stewartson layers has been found to be particularly significant in producing discrepancies between quasi-geostrophic theory without such layers and laboratory experiments run in the quasi-geostrophic regime (e.g. Mundt *et al.* 1995*a*; Mundt, Hart & Ohlsen 1995*b*). Unfortunately, the solid-body rotation velocity fields cannot be compared in the present setting. This is because although the velocity field is available from the numerical model, it is not available from the laboratory apparatus, which was configured specifically to measure interface height only.

Finally, it would be interesting to introduce a primitive equations model into the comparison, to explore more fully the essential non-quasi-geostrophic effects. For example, if part of the error in the quasi-geostrophic model were due to the filtering of inertia–gravity waves present in the laboratory, then a rotating shallow-water equations model should be capable of capturing it. Similarly, if part of the error were due to the large aspect ratio of the laboratory annulus, then a deep-water non-hydrostatic model should be capable of capturing it. Extensions to our study that involve the construction of bespoke primitive equations models are, therefore, attractive possible avenues for future work.

The general premise receiving support in our study, namely that quasi-geostrophic theory is useful for non-quasi-geostrophic parameter regimes, appears tangentially in several papers (e.g. Mundt *et al.* 1997) that focus on other topics. But the premise has not been explored systematically in a dedicated paper. Rather, it has entered into widespread belief without ever being tested comprehensively. If our findings are thought to be unsurprising, we contend that it will probably be based on unsupported conjecture rather than ideas deeply rooted in published work. We further contend that a dispassionate observer informed only by the existing literature could easily have expected much poorer agreement than we found. The success of quasi-geostrophic theory outside its formal bounds has been demonstrated and quantified herein, but the theoretical explanation remains to be elucidated.

We are grateful to three anonymous reviewers for their helpful comments and to Jim McWilliams and Hilary Weller for useful discussions. P. D. W. acknowledges funding through a University Research Fellowship from the Royal Society (reference UF080256) and a Fellowship from the Natural Environment Research Council (reference NE/D009138/1).

REFERENCES

Appleby, J. C. 1982 Comparative theoretical and experimental studies of baroclinic waves in a two-layer system. PhD thesis, University of Leeds.

Arakawa, A. 1966 Computational design for long-term numerical integration of the equations of fluid motion: two-dimensional incompressible flow. *J. Comput. Phys.* **1**, 119–143.

Bouchet, F. & Sommeria, J. 2002 Emergence of intense jets and Jupiter's Great Red Spot as maximum-entropy structures. *J. Fluid Mech.* **464**, 165–207.

Brugge, R., Nurser, A. J. G. & Marshall, J. C. 1987 A quasi-geostrophic ocean model: some introductory notes. *Tech Rep.* Blackett Laboratory, Imperial College.

Cattaneo, F. & Hart, J. E. 1990 Multiple states for quasi-geostrophic channel flows. *Geophys. Astrophys. Fluid Dyn.* **54**, 1–33.

Charney, J. G., Fjørtoft, R. & von Neumann, J. 1950 Numerical integration of the barotropic vorticity equation. *Tellus* **2** (4), 237–254.

Ekman, V. W. 1905 On the influence of the Earth's rotation on ocean currents. *Ark. Math. Astr. Fys.* **2**, 1–52.

Flierl, G. R. 1977 Simple applications of McWilliams' 'A note on a consistent quasigeostrophic model in a multiply connected domain'. *Dyn. Atmos. Oceans* **1**, 443–453.

Greenspan, H. P. 1968 *The Theory of Rotating Fluids*. Cambridge University Press.

Haltiner, G. J. & Williams, R. T. 1980 *Numerical Prediction and Dynamic Meteorology*, 2nd edn. Wiley.

Hart, J. E. 1972 A laboratory study of baroclinic instability. *Geophys. Fluid Dyn.* **3**, 181–209.

Hart, J. E. 1981 Wavenumber selection in nonlinear baroclinic instability. *J. Atmos. Sci.* **38** (2), 400–408.

Hart, J. E. 1995 Nonlinear Ekman suction and ageostrophic effects in rapidly rotating flows. *Geophys. Astrophys. Fluid Dyn.* **79**, 201–222.

Hart, J. E. & Kittelman, S 1986 A method for measuring interfacial wave fields in the laboratory. *Geophys. Astrophys. Fluid Dyn.* **36**, 179–185.

Hignett, P., White, A. A., Carter, R. D., Jackson, W. D. N. & Small, R. M. 1985 A comparison of laboratory measurements and numerical simulations of baroclinic wave flows in a rotating cylindrical annulus. *Quart. J. R. Meteorol. Soc.* **111**, 131–154.

King, J. C. 1979 Instabilities and nonlinear wave interactions in a two-layer rotating fluid. PhD thesis, University of Leeds.

Kwon, H. J. & Mak, M. 1988 On the equilibration in nonlinear barotropic instability. *J. Atmos. Sci.* **45** (2), 294–308.

Lewis, S. R. 1992 A quasi-geostrophic numerical model of a rotating internally heated fluid. *Geophys. Astrophys. Fluid Dyn.* **65**, 31–55.

Lovegrove, A. F. 1997 Bifurcations and instabilities in rotating two-layer fluids. PhD thesis, Oxford University.

Lovegrove, A. F., Read, P. L. & Richards, C. J. 2000 Generation of inertia–gravity waves in a baroclinically unstable fluid. *Quart. J. R. Meteorol. Soc.* **126**, 3233–3254.

McIntyre, M. E. 1967 Convection and baroclinic instability in rotating fluids. PhD thesis, Cambridge University.

McWilliams, J. C. 1977 A note on a consistent quasigeostrophic model in a multiply connected domain. *Dyn. Atmos. Oceans* **1**, 427–441.

McWilliams, J. C. 2007 Irreducible imprecision in atmospheric and oceanic simulations. *Proc. Natl Acad. Sci.* **104** (21), 8709–8713.

Mesinger, F. & Arakawa, A. 1976 Numerical methods used in atmospheric models. *Global Atmospheric Research Programme Publications Series No. 17*. World Meteorological Organization, Geneva.

Mundt, M. D., Brummell, N. H. & Hart, J. E. 1995*a* Linear and nonlinear baroclinic instability with rigid sidewalls. *J. Fluid Mech.* **291**, 109–138.

Mundt, M. D., Hart, J. E. & Ohlsen, D. R. 1995*b* Symmetry, sidewalls, and the transition to chaos in baroclinic systems. *J. Fluid Mech.* **300**, 311–338.

Mundt, M. D., Vallis, G. K. & Wang, J. 1997 Balanced models and dynamics for the large- and mesoscale circulation. *J. Phys. Oceanogr.* **27** (6), 1133–1152.

Pedlosky, J. 1964 The stability of currents in the atmosphere and the ocean. Part I. *J. Atmos. Sci.* **21**, 201–219.

Pedlosky, J. 1970 Finite-amplitude baroclinic waves. *J. Atmos. Sci.* **27**, 15–30.

Pedlosky, J. 1971 Finite-amplitude baroclinic waves with small dissipation. *J. Atmos. Sci.* **28**, 587–597.

Pedlosky, J. 1972 Limit cycles and unstable baroclinic waves. *J. Atmos. Sci.* **29**, 53–63.

Pedlosky, J. 1981 The nonlinear dynamics of baroclinic wave ensembles. *J. Fluid Mech.* **102**, 169–209.

Pedlosky, J. 1987 *Geophysical Fluid Dynamics*. Springer.

Phillips, N. A. 1954 Energy transformations and meridional circulations associated with simple baroclinic waves in a two-level, quasi-geostrophic model. *Tellus* **6** (3), 273–286.

Phillips, N. A. 1956 The general circulation of the atmosphere: a numerical experiment. *Quart. J. R. Meteorol. Soc.* **82** (352), 123–164.

Phillips, N. A. 1963 Geostrophic motion. *Rev. Geophys.* **1** (2), 123–176.

Read, P. L. 2001 Transition to geostrophic turbulence in the laboratory, and as a paradigm in atmospheres and oceans. *Surv. Geophys.* **22** (3), 265–317.

Read, P. L., Yamazaki, Y. H., Lewis, S. R., Williams, P. D., Wordsworth, R., Miki-Yamazaki, K., Sommeria, J. & Didelle, H. 2007 Dynamics of convectively driven banded jets in the laboratory. *J. Atmos. Sci.* **64** (11), 4031–4052.

Robert, A. J. 1966 The integration of a low order spectral form of the primitive meteorological equations. *J. Meteorol. Soc. Jpn* **44** (5), 237–245.

Smith, R. K. 1974 On limit cycles and vacillating baroclinic waves. *J. Atmos. Sci.* **31**, 2008–2011.

Smith, R. K. 1977 On a theory of amplitude vacillation in baroclinic waves. *J. Fluid Mech.* **79** (2), 289–306.

Smith, R. K. & Pedlosky, J. 1975 A note on a theory of vacillating baroclinic waves *and* Reply. *J. Atmos. Sci.* **32**, 2027.

Stewartson, K. 1957 On almost rigid rotations. *J. Fluid Mech.* **3**, 17–26.

White, A. A. 1986 Documentation of the finite difference schemes used by the Met O 21 two-dimensional Navier–Stokes model. *Tech Rep.* Met O 21 IR86/3. Geophysical Fluid Dynamics Laboratory, UK Meteorological Office.

Williams, G. P. 1979 Planetary circulations. Part 2. The Jovian quasi-geostrophic regime. *J. Atmos. Sci.* **36**, 932–968.

Williams, P. D. 2003 Nonlinear interactions of fast and slow modes in rotating, stratified fluid flows. PhD thesis, Oxford University. http://ora.ouls.ox.ac.uk/objects/uuid:5365c658-ab60-41e9-b07b-0f635909835e.

Williams, P. D., Haine, T. W. N. & Read, P. L. 2004*a* Stochastic resonance in a nonlinear model of a rotating, stratified shear flow, with a simple stochastic inertia–gravity wave parameterization. *Nonlin. Proc. Geophys.* **11** (1), 127–135.

Williams, P. D., Haine, T. W. N. & Read, P. L. 2005 On the generation mechanisms of short-scale unbalanced modes in rotating two-layer flows with vertical shear. *J. Fluid Mech.* **528**, 1–22.

Williams, P. D., Haine, T. W. N. & Read, P. L. 2008 Inertia–gravity waves emitted from balanced flow: Observations, properties, and consequences. *J. Atmos. Sci.* **65** (11), 3543–3556.

Williams, P. D., Haine, T. W. N., Read, P. L., Lewis, S. R. & Yamazaki, Y. H. 2009 QUAGMIRE v1.3: a quasi-geostrophic model for investigating rotating fluids experiments. *Geosci. Model Develop.* **2** (1), 13–32.

Williams, P. D., Read, P. L. & Haine, T. W. N. 2004*b* A calibrated, non-invasive method for measuring the internal interface height field at high resolution in the rotating, two-layer annulus. *Geophys. Astrophys. Fluid Dyn.* **98** (6), 453–471.

Zurita-Gotor, P. & Vallis, G. K. 2009 Equilibration of baroclinic turbulence in primitive equations and quasigeostrophic models. *J. Atmos. Sci.* **66**, 837–863.